

Jan Hricák, [jan.hricak@fsv.cvut.cz](mailto:jan.hricak@fsv.cvut.cz)

WG3 - Michal Jandera, [michal.jandera@fsv.cvut.cz](mailto:michal.jandera@fsv.cvut.cz)

WG2 - František Wald, [wald@fsv.cvut.cz](mailto:wald@fsv.cvut.cz)

### **3 LOCAL BUCKLING OF CLASS 4 SECTIONS AT ELEVATED TEMPERATURE**

#### Summary

A significant progress in fire engineering research was made in the last decade. This resulted in more precise structural fire design and higher reliability of steel structures. However, for design of very slender sections (Class 4 cross-sections according to the Eurocode 3), where elevated temperature affects also behaviour of elements subjected to local buckling, no wide research was published.

This article describes the course of the experiment and validation of a numerical model based on the data obtained.

#### **3.1 INTRODUCTION**

A common practice in recent years, thanks to the introduction of European design standards for building construction has become not only an assessment of the structure at normal design situation, but also in the fire (Buchanan, 2001), (CEN, 2001). The area of slender cross-sections research is very important, because the assessment and design principles of Class 4 cross-sections are very specific and usually more difficult than for normal cross-sections. Along with any global problems their behaviour includes also local buckling of the compressed parts of the cross-section (Trahair, 2001), (CEN, 2004).

The research is focused on the behaviour of steel beams made from welded class 4 cross sections of I and H shape exposed to high temperatures.

#### **3.2 DESIGN AND EXECUTION OF EXPERIMENTS**

The focus of the project is to carry out experiments with I - beams with slender cross-sections, which belong to the Class 4. The load capacity of these sections is not directly affected by the yield strength of the steel, but by deformations of the compressed areas of the cross-section, i.e. upper part the web and the upper flange. It was necessary to choose the appropriate cross-sectional shape to reach this way of the deformation of the samples during the planned experiments, beam load form and force. Four tests with two types of cross-section loaded by four-point bending were be carried out. (see Fig. 3.1).

Beams were heated to a constant temperature by an electric heating pads. Increasing load was applied until exhaustion of the load capacity. Each section was heated to a temperature of 450 °C and 650 °C. These experiments were complemented by a number of material tests at normal temperature.

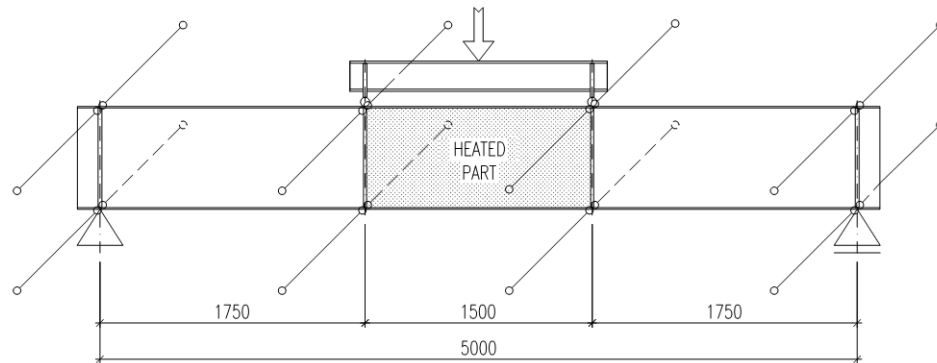


Fig. 3.1 Static scheme of the experiment

For these experiments, there were two types of welded cross-sections chosen. They represent Class 4 cross-sections and they are sufficiently burdened by the problematic of local stability of the walls.

- The Cross-Section A (IW 680/250/12/4) has the web in the Class 4 and the flanges are in Class 3, see Fig. 3.2a.
- The Cross-Section B (IW 846/300/8/5) has the web in the Class 4 and the flanges are in Class 4, see Fig. 3.2b.

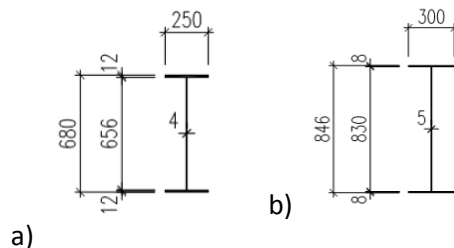


Fig. 3.2 Cross sections designed for experiment: a) Cross-section A, b) Cross-section B

Steel test fixtures were designed and manufactured to ensure smooth running of the experiment and proper introduction of all the boundary conditions according to the static scheme (see Fig. 3.1). steel test fixtures were designed and manufactured. The scheme of the test fixtures layout including the location of the test beam is shown in the following figure (see Fig. 3.3).

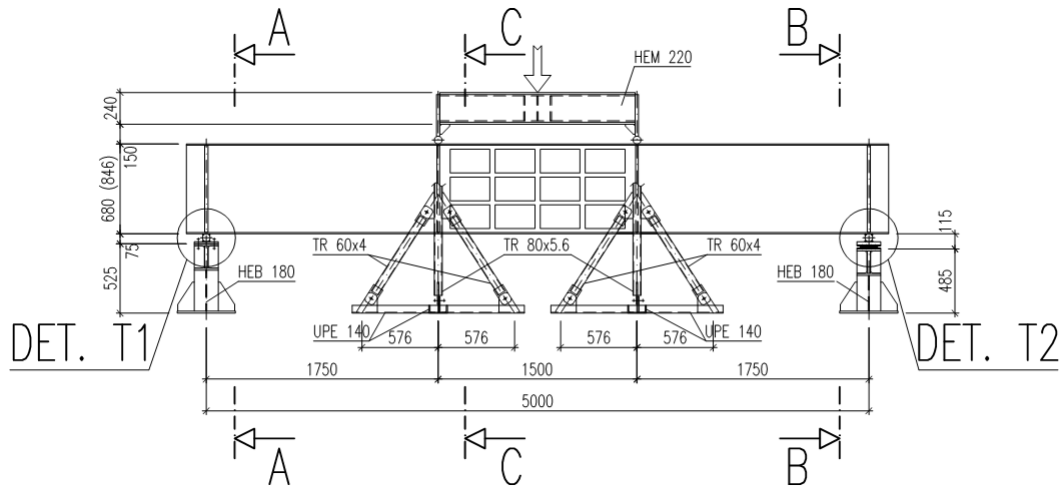


Fig. 3.3 Scheme of the experiment set-up

### 3.2.1 The test fixtures for ensuring the torsional stability

The principle of the test fixtures for ensuring the torsional stability at the support points and at the point of the load input is shown in the section views A-A, B-B and C-C (see Fig. 3.4).

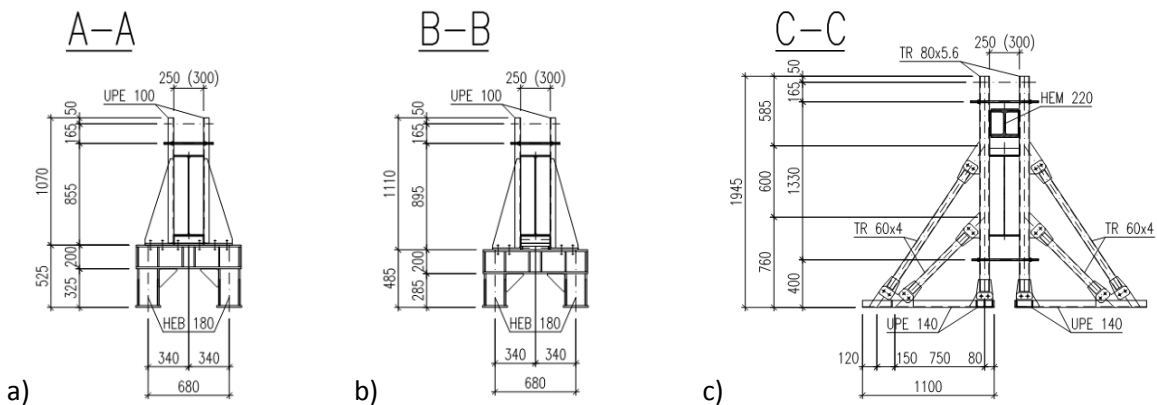


Fig. 3.4 Sections: a) at the point of the firm joint support, b) at the point of the sliding joint support, c) at the point of the load introduction

The construction of the test fixtures at the support (see Fig. 3.4a, b) is formed by two vertical guide profiles. The test fixtures for ensuring the torsion stability at the point of the load introduction (see Fig. 3.4c) are formed by the struts, which hold a vertical pair of guide profiles. After placing the test beam to the support, the individual test fixtures will clamp the cross-section of the beam with a small allowance, therefore free movement in the vertical and longitudinal directions is not obstructed, but the lateral and the torsional stability was ensured.

### 3.2.2 The design of the supports

The test beams were, according to the scheme (see Fig. 3.3), placed on the fixed articulated support from the left side (see Fig. 3.5a) and on the sliding joint support (see Fig. 3.5b) from the right side. The sliding articulated support is designed as a rolling bearing.

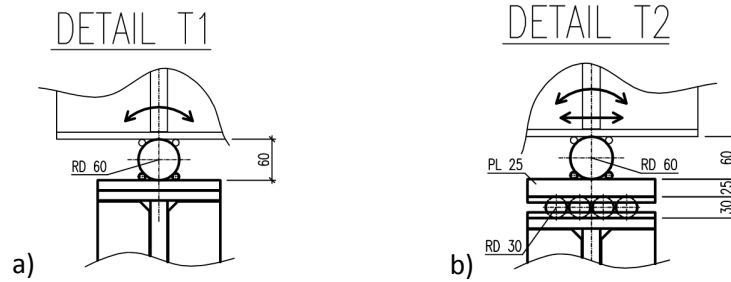


Fig. 3.5 Construction detail: a) Fixed articulated support, b) Sliding articulated support

### 3.3 Measurement of imperfections of the beams

Values of imperfections were determined by manual measurements in a precisely defined grid (see Fig. 3.6). The values of individual readings are shown in the graphs (see Figs. 3.7-3.10). The maximal amplitudes were chosen from the summary of the readings (see Tab. 3.1).

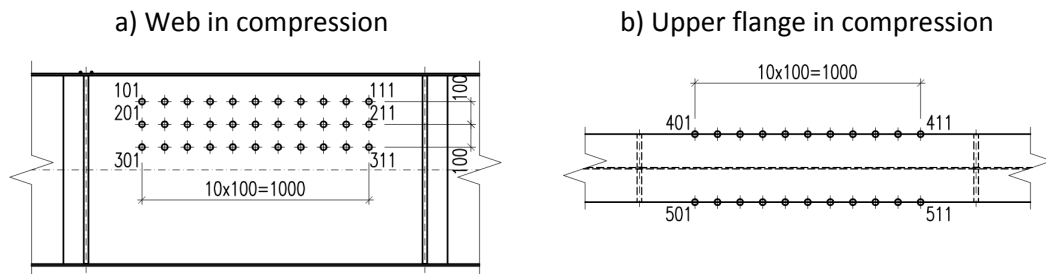


Fig. 3.6 Defined grid of in the central heated part of the beam

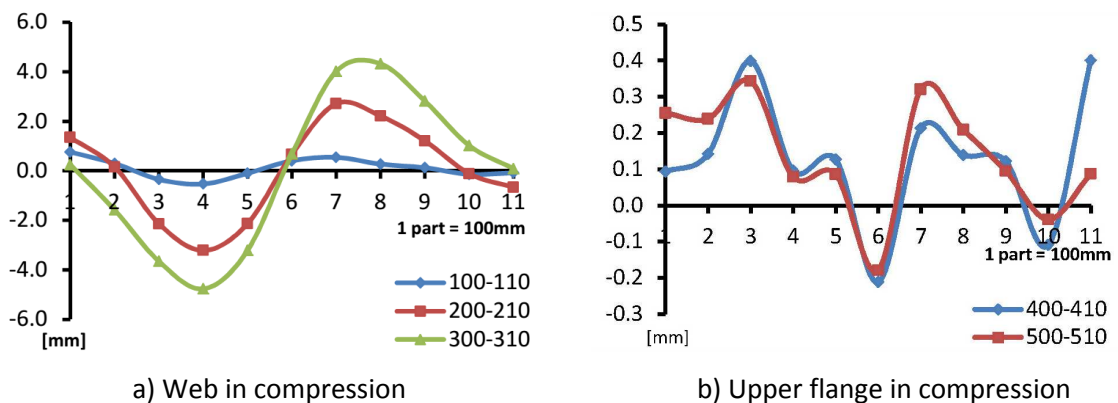


Fig. 3.7 Changing the amplitude imperfections for beam A1 (IW 680/250/12/4)

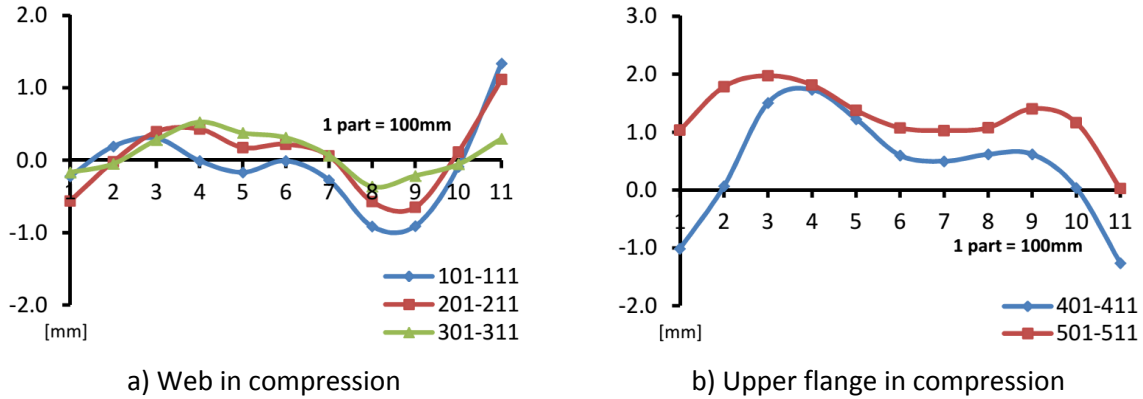


Fig. 3.8 Changing the amplitude imperfections for beam A2 (IW 680/250/12/4)

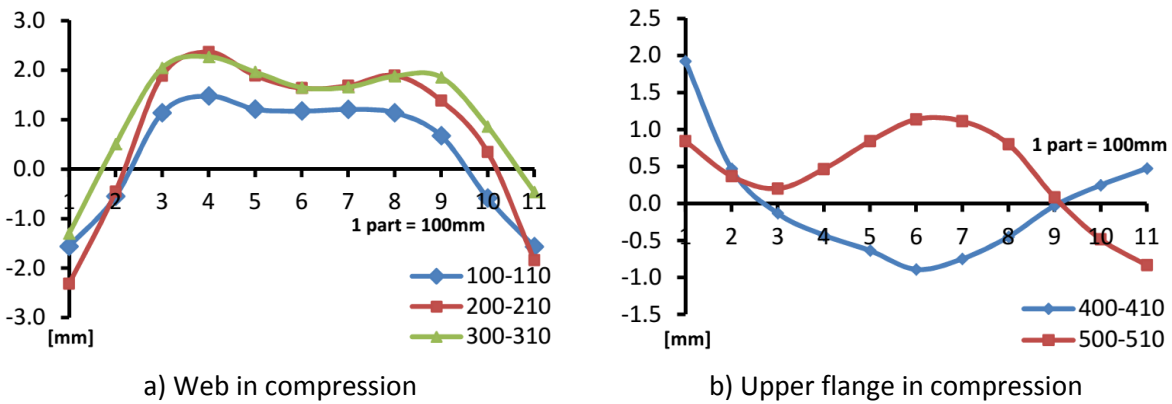


Fig. 3.9 Changing the amplitude imperfections for beam B1 (IW 846/300/5/8)

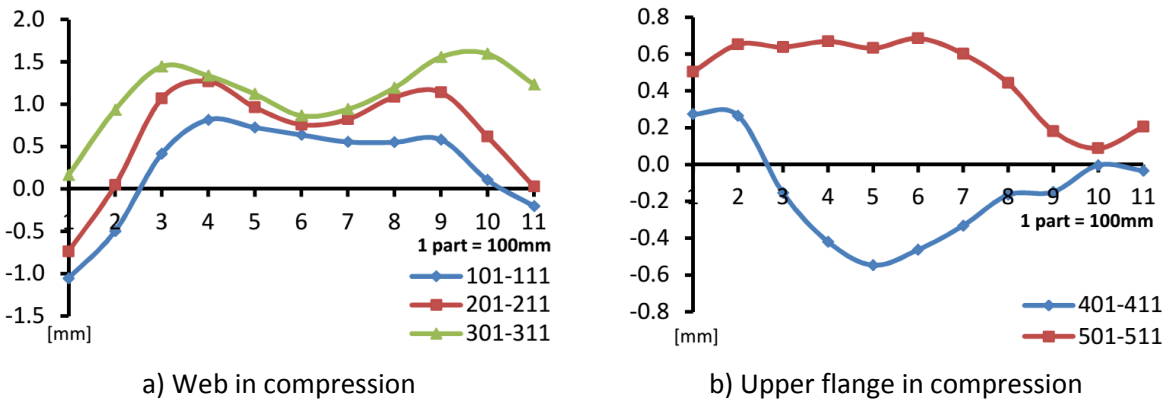


Fig. 3.10 Changing the amplitude imperfections for beam B2 (IW 846/300/5/8)

Tab. 3.1 Maximum amplitudes of the imperfection from the manual measurement

Beam	Cross-Section	Web [mm]	Flange [mm]
A1	A (IW 680/250/4/12)	4.765	1.200
A2	A (IW 680/250/4/12)	1.340	1.975

B1	B (IW 846/300/5/8)	2.364	1.924
B2	B (IW 846/300/5/8)	1.595	0.685

### 3.4 PROGRESS OF THE EXPERIMENT

After connecting all sensing devices (thermocouples, potentiometers, dynamometer in a hydraulic jack) to the central measuring equipment and after connection of the heating pads to the transformer, the beam was ready for the experiment (see Fig. 3.11).

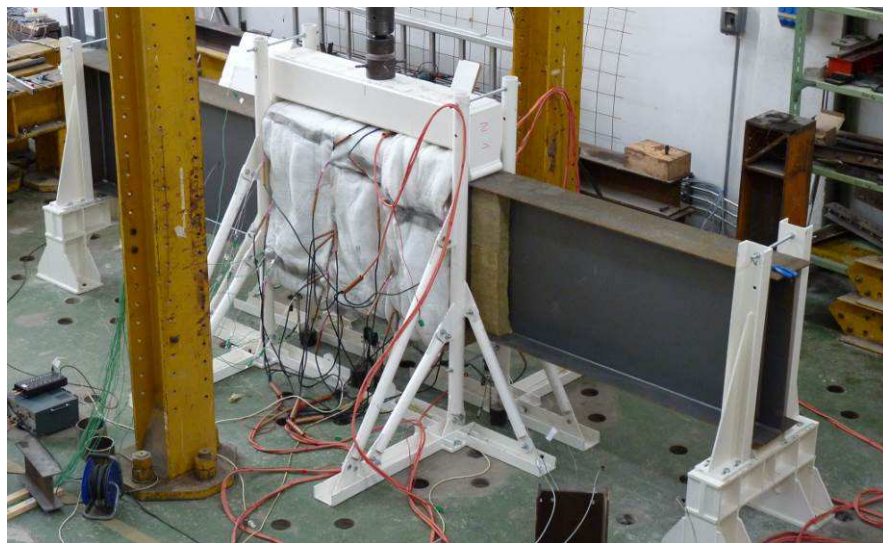


Fig. 3.11 The prepared test beam prior the experiment

Warm-up time for the temperature  $T \approx 450 \text{ }^\circ\text{C}$  was  $\sim 45$  minutes and  $\sim 65$  minutes for the temperature  $T \approx 650 \text{ }^\circ\text{C}$ . After reaching the desired temperature in the heated part of the beam, the application of the mechanical loading was started. The hydraulic jack, which was controlled by a constant proportion of the deflection path in the middle part of the heated beam, was affecting the test beam through the load beam. The test beam was thus loaded by four-point bending. The following load-deflection diagrams for Tests 1-4 (see Fig. 3.12) show the dependence of the applied load and the deflection in the middle of the heated part of the test beam. Summary of the results is shown in Tab. 3.2.

The behaviour of proposed Class 4 cross-sections in the experiments corresponded to expectations and there was significant buckling of the compressed part of the section observed, see Figs. 3.18 b, 3.19 b, 3.21b and 3.22b.

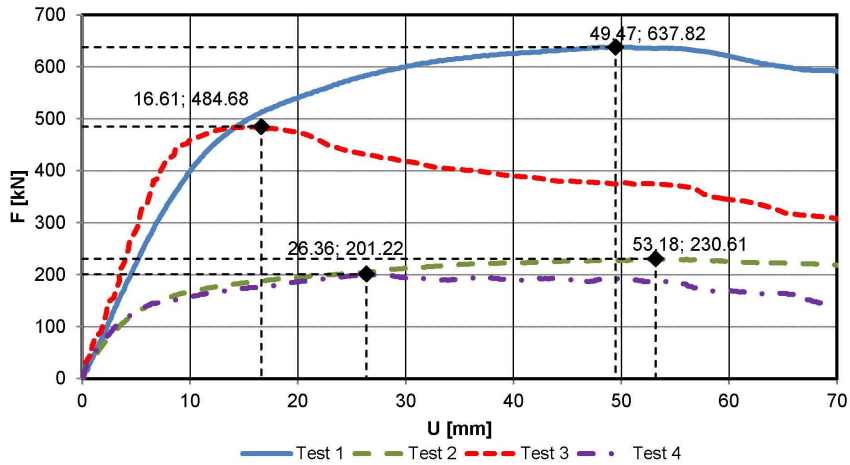


Fig. 3.12 Load-deflection diagram for Tests 1-4

Tab. 3.2 Load capacity of the Test beams

Test	Cross-Section	Temperature [°C]	Load capacity [kN]
1	A1 (IS 680/250/4/12)	~ 450	637
2	A2 (IS 680/250/4/12)	~ 650	230
3	B1 (IS 846/300/5/8)	~ 450	484
4	B2 (IS 846/300/5/8)	~ 650	201

### 3.5 NUMERICAL SIMULATION OF EXPERIMENTS

This part of the study includes description of a numerical model created by a finite element method (FEM) and its validation. The numerical model was created in ABAQUS software (ABAQUS, 2010). The model was compared to the experiments. It should be noted that the influence of residual stress is not included in the analysis.

#### 3.5.1 Meshing of the beams

It is advantageous to use shell elements for the modelling of thin-walled elements. These elements are suitable for the wall of the slenderness of more than 10 (the width / thickness ratio). Element S4 (see Fig. 3.13) was used for the comparative study of the shell elements.

The shell element S4 has four nodes with six degrees of freedom (three displacements and three rotations), linear approximations and full integration (4 integration points on the surface of the element). Element S4 can be used in the calculation of large deformations and large rotations. For each model of the beam, web is formed by 200 elements along the length and by 16 elements along the

height of the cross-section. Upper and lower flanges are formed by 6 elements along the width of the cross-section. The structural mesh is shown in Fig 3.16.

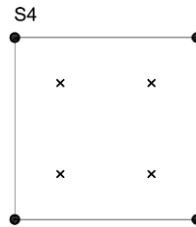


Fig. 3.13 Shell element S4

### 3.5.2 Geometric imperfections

After set-up of the experiment, initial imperfections in the heated part of the beam were measured as described above (see paragraph 3.3). Initial imperfections were entered for the numerical model to correspond the real beams from the experiments. The individual curves describing the shape imperfections (see Figs. 3.7 - 3.10) were replaced by a sinusoidal function for simplification with the maximum amplitude taken from Tab. 3.1.

### 3.5.3 Material modelling

Mechanical properties of steel at normal temperature were determined from the mechanical tests for each thickness of the plate. Mechanical properties at high temperatures were obtained with the help of the reduction factors dependent on temperature, which are listed in EC 3 Part 1- 2 (CEN, 2004). Material behaviour at high temperature is defined by the elastic-plastic non-linear stress-strain relationship (see Fig. 3.15). Mechanical properties (yield stress and modulus of elasticity) for the individual plates according to the scheme (see Fig. 3.14) are shown in the Tab. 3.3.

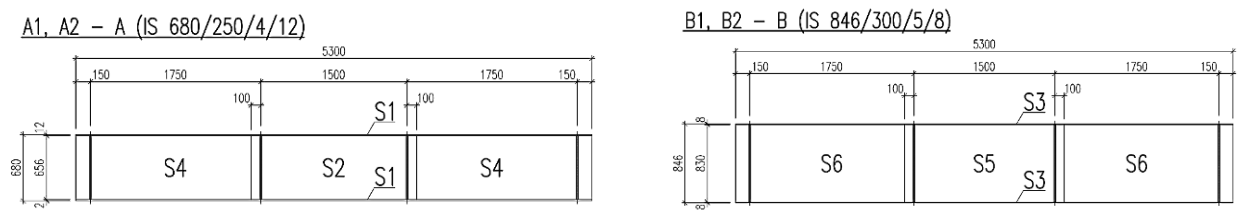


Fig. 3.14 Layout scheme of each plate

Tab 3.3 Material properties for the individual plates

Part	[MPa]	S1	S2	S3	S4	S5	S6
Upper Yield Stress	$R_{eH}$	430	394	341	376	385	435
Lower Yield Stress	$R_{eL}$	424	391.67	338	361	378	408
Elastic Modulus	E	178399	176897	194375	199200	209988	208900

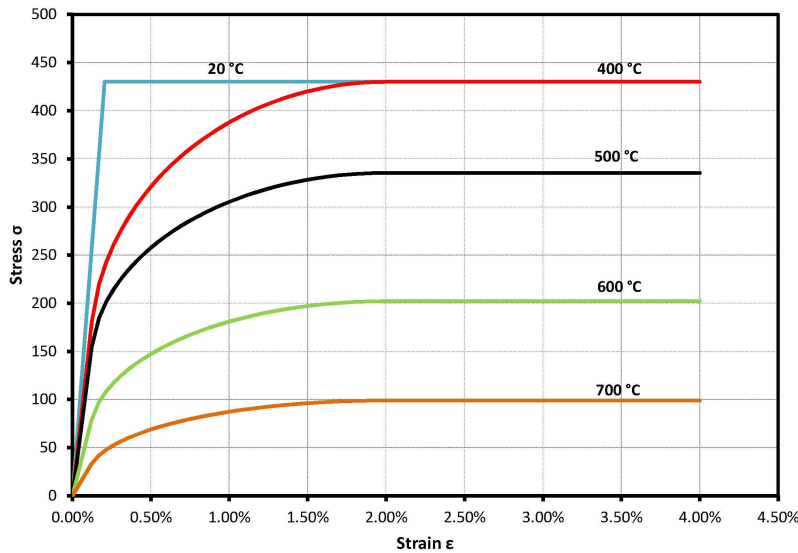


Fig. 3.15 Stress–strain relationship for S1

### 3.5.4 Boundary conditions and loading

For the simulation of the boundary conditions according to the static scheme (see Fig. 3.1), the fixed articulated support was chosen on the left side of the model (the point "a") and the sliding articulated support was chosen on the right side (the point "d"), see Fig. 3.16. On the left side, shift in the direction of the X, Y, Z axis and the rotation about the X axis are blocked, the rotation about the Z axis is not restrained. On the right side, the shift in the direction of the Y, Z axis and rotation about the X axis are blocked, the shift in the direction of the X axis and the rotation about the Z axis are not restrained. In the point of the load application (the points "b", "c"), shift in the direction of the Z axis is blocked, shift in the direction of the X and Y axes is not restrained.

The static structural analyses (load–displacement analysis) were performed to predict the load–deflection behaviour of the steel beams. Regarding the application of load, the two concentrated loads were applied incrementally by means of equivalent displacements to overcome convergence problems and to facilitate the capture of the post-buckling behaviour of the models. Displacement loads were applied at 1/3 span of the steel beams (see Fig. 3.1) and the load step increments were varied in order to avoid potential numerical problems. The region between the two loading points (L = 1500 mm) is the tested part where uniform bending moment acts. Loading points are shown in Fig. 3.16.

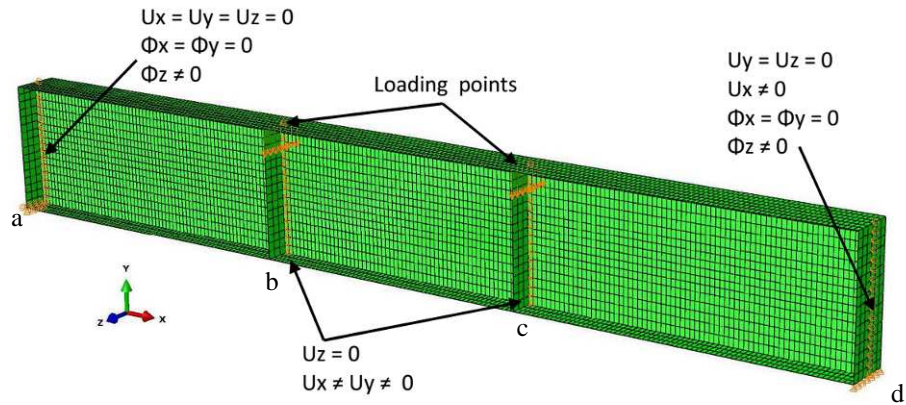


Fig. 3.16 Loading and boundary conditions for beams

### 3.5.5 Steel temperature distribution in numerical modelling

The real temperatures attained in steel cross sections during the experiments were evenly introduced at each node of the heated part of the shell elements in the finite element structural models. The following data provide the distribution of temperature used for the numerical simulations, see Fig. 3.17 and Tab. 3.4.

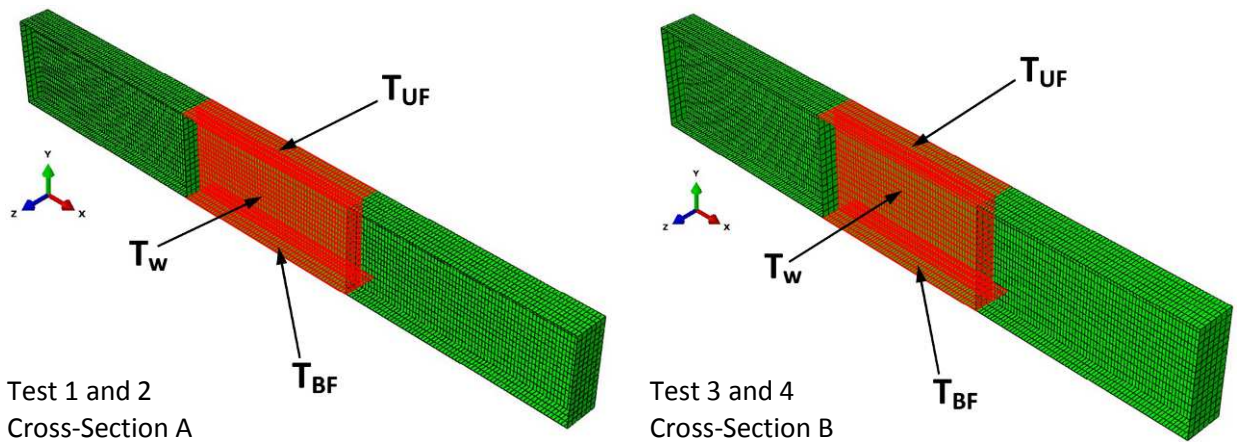


Fig. 3.17 Temperature distribution in numerical model

Tab 3.4 Temperatures for Tests 1-4

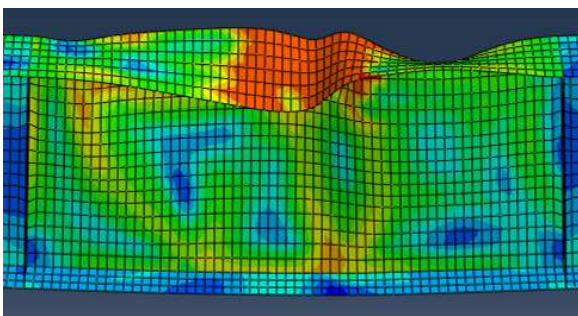
T [°C]	A (IW 680/250/4/12)		B (IW 846/300/5/8)	
Test	1	2	3	4
$T_{UF}$	444	654	481	661
$T_{BF}$	469	636	425	631
$T_w$	458	649	431	641

### 3.6 RESULTS OF THE NUMERICAL SIMULATION vs. TEST RESULT

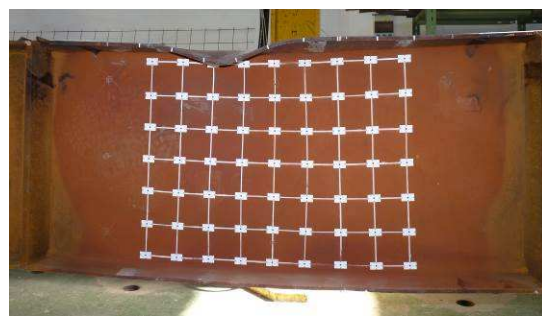
In the next table and figures, the results obtained in the fire tests are compared to the results obtained in the numerical simulations. Failure mode of the tests and the numerical model is also compared in the figures.

#### 3.6.1 Model for Test 1 and Test 2 (IS 680/250/4/12)

The following figures (Fig. 3.18 and 3.19) show the deformed shape of the central heated part of the beam from the numerical simulation and from the experiment for Test 1 and Test 2.

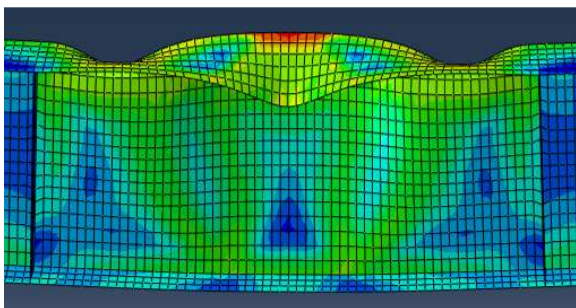


a) Numerical simulation



b) Experiment

Fig. 3.18 Deformed shape for Test 1



a) Numerical simulation



b) Experiment

Fig. 3.19 Deformed shape for Test 2

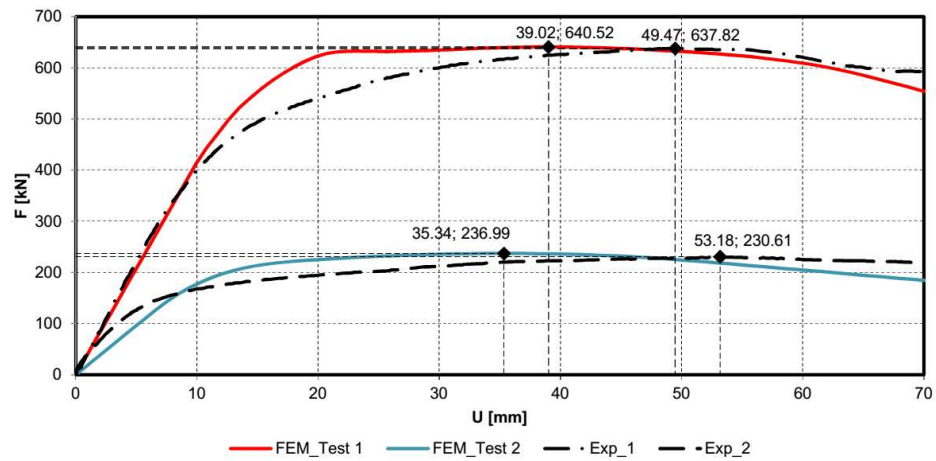
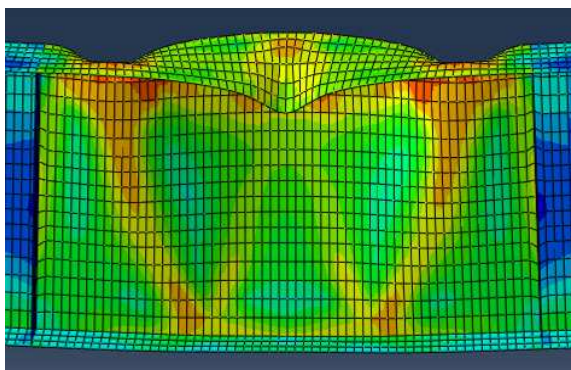


Fig. 3.20 Load-deflection diagram for Test 1 and 2

### 3.6.2 Model for Test 3 and Test 4 (IS 846/300/5/8)

Figs. 3.21 and 3.22 show the deformed shape from the numerical simulation and from the experiment for Test 3 and Test 4.

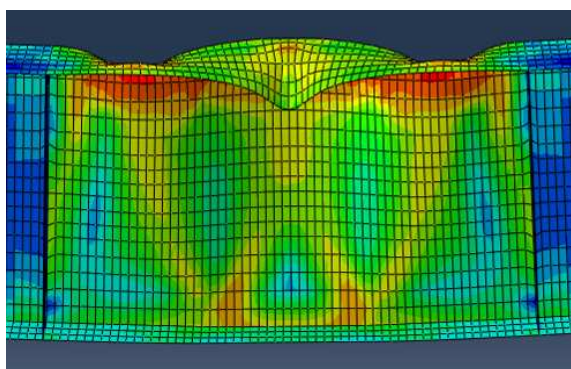


a) Numerical simulation



b) Experiment

Fig. 3.21 Deformed shape for Test 3 and 4



a) Numerical simulation



b) Experiment

Fig. 3.22 Deformed shape for Test 3

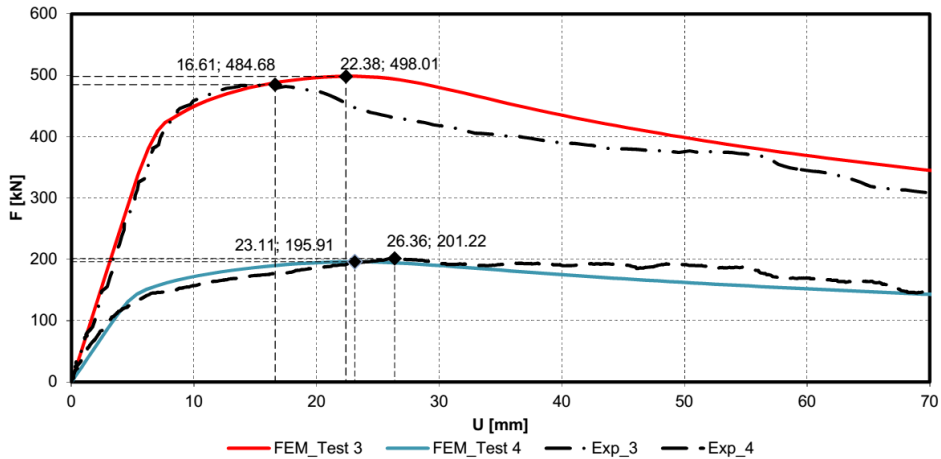


Fig. 3.23 Load-deflection diagram for Test 3 and 4

### 3.6.3 Comparison

The following table and figure summarize the numerical results and compare them to the test results.

Tab. 3.5 Summary of tests results vs. numerical results

Test	Cross-Section	Load capacity [kN]		$\epsilon$ [%]
		Experiment	FEM	
1	A1 (IS 680/250/4/12)	637.82	640.52	0.42
2	A2 (IS 680/250/4/12)	230.61	236.99	2.69
3	B1 (IS 846/300/5/8)	484.68	498.01	2.68
4	B2 (IS 846/300/5/8)	201.22	195.91	2.64

### 3.7 CONCLUSION

Numerical simulations exhibit similar behaviour as the test beams in the experiment. As seen in Tab. 3.5 and Fig. 3.24, the difference between the results of numerical model in ABAQUS and ultimate resistance obtained from the experiment is smaller than 3%. Therefore, we can say that the material model at high temperatures is suitable for creating numerical simulation of steel beams with Class 4 cross-sections exposed to fire.

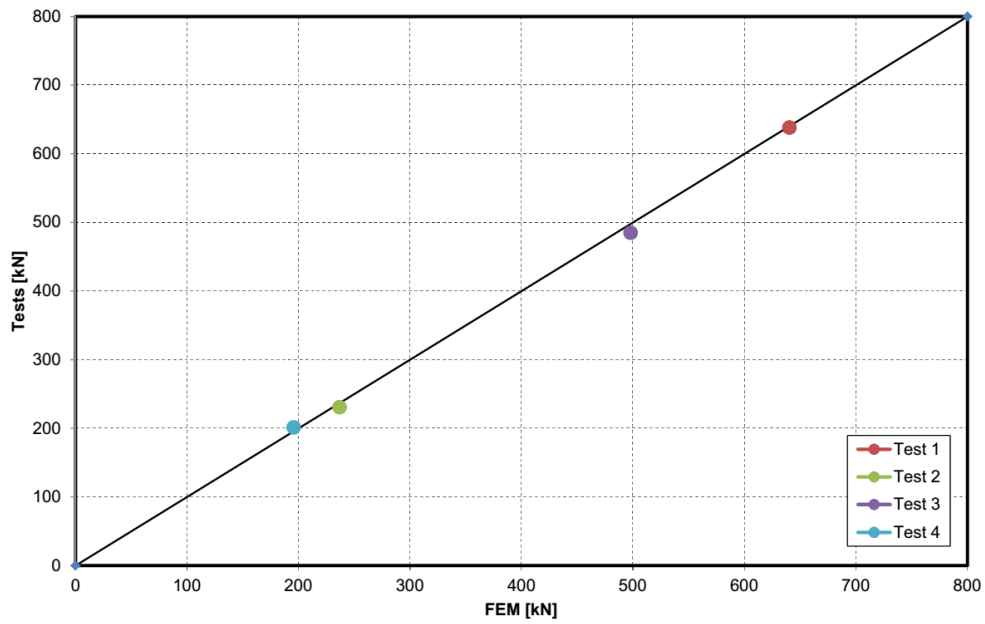


Fig. 3.24 Comparison of test results with numerical results

### References

- Buchanan, 2001: Buchanan A. H., Structural Design for Fire Safety, New Zealand, 2001.
- Trahair, 2001: Trahair, N. S., Bradford, M. A., Nethercot, D. A., The Behaviour and Design of Steel Structures, London, 2001.
- CEN, 2001: CEN. Eurocode 3: design of steel structures, part 1.2: general rules—structural fire design (EN 1993-1-2:2001). Brussels: European Committee for Standardization; 2001.
- CEN, 2004: CEN. Eurocode 3: design of steel structures, part 1.5: plated structural elements (EN 1993-1-5:2004). Brussels: European Committee for Standardization; 2004.
- ABAQUS, 2010: Analysis user's manual, Volumes I-IV, version 6.10. (2010). Hibbitt, Karlsson & Sorenses, Inc., Providence, R.I, USA.